



Perspectives on Small Animal Radionuclide Imaging; Considerations and Advances in Atherosclerosis

Eric J. Meester^{1,2}, B. J. Krenning³, J. de Swart¹, M. Segbers¹, H. E. Barrett^{1,2}, M. R. Bernsen¹, K. Van der Heiden² and Marion de Jong^{1*}

¹ Department of Radiology and Nuclear Medicine, Erasmus Medical Center, Rotterdam, Netherlands, ² Department of Biomedical Engineering, Thorax Center, Erasmus Medical Center, Rotterdam, Netherlands, ³ Department of Cardiology, Thorax Center, Erasmus Medical Center, Rotterdam, Netherlands

OPEN ACCESS

Edited by:

Francesco Cicone,
Lausanne University Hospital (CHUV),
Switzerland

Reviewed by:

Gaurav Malviya,
University of Glasgow,
United Kingdom
Antti Saraste,
University of Turku, Finland
Fabien Hyafil,

Assistance Publique Hopitaux De
Paris (AP-HP), France

*Correspondence:

Marion de Jong
m.hendriks-dejong@erasmusmc.nl

Specialty section:

This article was submitted to
Nuclear Medicine,
a section of the journal
Frontiers in Medicine

Received: 21 November 2018

Accepted: 11 February 2019

Published: 11 March 2019

Citation:

Meester EJ, Krenning BJ, de Swart J, Segbers M, Barrett HE, Bernsen MR, Van der Heiden K and de Jong M (2019) Perspectives on Small Animal Radionuclide Imaging: Considerations and Advances in Atherosclerosis. *Front. Med.* 6:39.
doi: 10.3389/fmed.2019.00039

This review addresses nuclear SPECT and PET imaging in small animals in relation to the atherosclerotic disease process, one of our research topics of interest. Imaging of atherosclerosis in small animal models is challenging, as it operates at the limits of current imaging possibilities regarding sensitivity, and spatial resolution. Several topics are discussed, including technical considerations that apply to image acquisition, reconstruction, and analysis. Moreover, molecules developed for or applied in these small animal nuclear imaging studies are listed, including target-directed molecules, useful for imaging organs or tissues that have elevated expression of the target compared to other tissues, and molecules that serve as substrates for metabolic processes. Differences between animal models and human pathophysiology that should be taken into account during translation from animal to patient as well as differences in tracer behavior in animal vs. man are also described. Finally, we give a future outlook on small animal radionuclide imaging in atherosclerosis, followed by recommendations. The challenges and solutions described might be applicable to other research fields of health and disease as well.

Keywords: mice, nuclear imaging, SPECT, PET, atherosclerosis

INTRODUCTION

Small Animal Radionuclide Imaging

Nuclear imaging using Single Photon Emission Computed Tomography (SPECT) or Positron Emission Tomography (PET) allows high-sensitivity and (semi-) quantitative imaging of physiological processes or molecular targets *in vivo*. Before clinical application, preclinical evaluation of novel radiotracers is a requisite to assess tracer characteristics such as *in vivo* tracer kinetics, target specificity, stability, and biodistribution. This is greatly facilitated by the widespread use of small animal models of disease as well as the development of state of the art small animal SPECT and PET systems, which allow tracer examination up to sub-mm resolution (1–6). However, preclinical nuclear imaging of small animals comes with a particular set of challenges and opportunities different from clinical nuclear imaging.

Atherosclerosis

The challenges and opportunities of small animal imaging become apparent in e.g., atherosclerosis imaging. Atherosclerosis is an inflammatory disease in which fatty plaques might occlude an artery through continued lipid deposition or sudden rupture of vulnerable plaques. Occlusion of an artery can lead to myocardial infarction, stroke, or limb ischemia. Early detection and characterization of atherosclerosis is therefore important, but remains problematic. Many imaging techniques such as contrast enhanced Computed Tomography (CT) focus on degree of stenosis, but fail to identify vulnerable plaques. Functional imaging of biological processes involved in plaque development or progression may identify and localize plaques at risk of rupture. Moreover, the characteristics of a vulnerable plaque, such as the presence of intraplaque hemorrhage, a large influx of inflammatory cells, neovessel formation, or a thin fibrous cap (7), provides ample possibilities for nuclear imaging. Yet, when studying novel tracers that might fulfill this need, research teams are faced with challenges. Differences between animal models of atherosclerosis and the human pathophysiology can make imaging results difficult to interpret. Furthermore, the small size of the plaques in small animal models, as well as the low and diffuse density of targets in a plaque, can severely complicate the evaluation process including quantification options *in vivo*.

Nuclear Imaging of Atherosclerosis

2-deoxy-2-[¹⁸F]fluoro-D-glucose ([¹⁸F]FDG) has been extensively studied for the detection and quantification of inflammatory cells in atherosclerosis (8, 9), and has been shown an independent predictor of recurrent events after stroke (10–12). Moreover, differentiation between different plaque phenotypes in the carotid arteries was successfully investigated using this tracer (13). However, unspecific uptake of [¹⁸F]FDG, especially in the metabolically active myocardium, limits its use to detect plaques in coronary arteries. As such more specific tracers are urgently needed.

In this review, we describe small animal radionuclide imaging with a strong focus on applications in atherosclerosis. We discuss differences between the pathophysiology of human and mouse atherosclerosis, related technical aspects, and challenges of small animal radionuclide imaging, as well as atherosclerosis tracer development and evaluation. Moreover, we discuss the future outlook and give recommendations.

CONSIDERATIONS ON MODELS OF ATHEROSCLEROSIS

Animal Models of Atherosclerosis

A number of atherosclerotic animal models have been developed, as reviewed in Getz and Reardon (14). In short, porcine and primate models resemble human atherosclerosis best, yet are costly to maintain and are less established with regard to genetic modification. The plaques in rabbit models resemble human plaque less, as rabbit plaques mainly contain lipids. Rabbit models have certain advantages over mouse models,

including the diameter of the abdominal aorta being similar to human coronary arteries and less subjected to movement. However, rabbit models are less frequently used since the introduction of the Apolipoprotein E deficient (ApoE^{-/-}) and low density lipoprotein receptor knock-out (LDLR^{-/-}) (KO) mouse models (15). Most atherosclerosis studies therefore use murine models, as mouse plaques develop faster than rabbit plaques, the mouse models are well-characterized, have low costs, and are widely available. Recent developments like clustered regularly interspaced short palindromic repeats/Cas9 (CRISPR/Cas9) targeted genome editing to create KOs (16), and pro-protein convertase subtilisin/kexin type 9 (PCSK9) injection to rapidly induce atherosclerosis (17), have created new opportunities in modeling human-like atherosclerotic disease in mice. We refer to Veseli et al. (18) for a more extensive review of mouse models of atherosclerosis. Besides advantages in using atherosclerotic mice, there are several considerations to be taken into account when choosing a mouse model and interpreting imaging results.

Plaque Location and Composition

Like in humans, atherosclerosis in mice is multifocal and locates in specific regions of the vasculature, determined by the hemodynamic environment (19). Pre-clinical imaging studies generally study plaques located in the inner curve of the aorta, the carotid arteries, and brachiocephalic artery, while translating their results to human coronary disease. Plaque composition as well as plaque stability or vulnerability differ between mice and men; differences in lipid metabolism lead to different lipid profiles related to the ratio between high, very low, and low density lipoprotein (HDL, VLDL, and LDL) (14, 20). Moreover, thin caps or intraplaque hemorrhage are rare in traditional mouse models, whereas they are characteristic of human vulnerable atherosclerosis (21), and plaque rupture is rarely seen in commonly used mouse models (22). To create a mouse model with plaque rupture, double knock outs (23, 24) or invasive experimental interventions are required, which arguably do not mimic human plaque rupture mechanisms (25).

Immune Subsets

Inflammatory cells are often used as imaging targets, because of the important role they have in plaque formation and progression. Yet, it is reported that human and mouse macrophage subsets differ (26, 27), which therefore makes validation in human tissue necessary.

Despite these differences between human and murine atherosclerosis, mice are valuable in testing radiotracers, as processes like angiogenesis and inflammation are present in mouse plaques. Therefore, mice can be used for proof of concept studies, or to assess tracer behavior *in vivo*. Moreover, *ex vivo* validation by gamma-counting, autoradiography, and immunohistochemistry allows better quantification of radiotracers. However, for reasons discussed above, translating results obtained in mouse models to expect human results should be done with caution.

TECHNICAL DEVELOPMENTS AND APPLICATIONS IN SMALL ANIMAL RADIONUCLIDE IMAGING

Nuclear Imaging of Mouse and Human Plaques

SPECT and PET can both provide very high sensitivity, even suitable for imaging of very small quantities of radiotracers (nM-pM range), enabling investigation of specific cells or pathophysiological processes. Developments in these systems for small animal imaging and in processing of imaging data allow better examination of novel radiotracers. Moreover, preclinical systems allow high resolution and sensitive examination of human tissues (28, 29). When imaging mouse atherosclerosis challenges become apparent: high spatial resolution is crucial in small murine plaques. The largest murine plaques are located in the aorta, which has a diameter of ~1 mm. High sensitivity is however also very important, as these small plaques contain relatively few target cells, on which receptor expression can be low compared to other disease models such as tumor models.

Here we highlight a number of developments in imaging and image processing, see (30–36) for more extensive reviews on nuclear imaging methods.

Preclinical SPECT

SPECT systems require a collimator to obtain directional information on gamma rays emitted from within the animal or patient sample to be imaged. Traditional clinical SPECT systems generally use a parallel hole collimator, which limits resolution and sensitivity in comparison to clinical PET systems that do not require a collimator (Table 1) (44). The choice of collimator heavily depends on the imaging task at hand because of the classic trade-off between resolution and sensitivity in collimator design. Regarding spatial resolution, major improvements have been made in preclinical SPECT by the introduction of pinhole cameras, in which magnified projection data can be acquired by choosing the right positions of the pinholes between the scintillation crystal and the animal (45), enabling sub-mm resolutions (Table 1 and Figure 1). Such high spatial resolutions can be achieved by decreasing the diameter of the pinhole, but

TABLE 1 | Shows a tabulated overview of properties of clinical and preclinical PET and SPECT.

	Small Animal Scanners		Standard Clinical Scanners	
	Resolution [mm]	Sensitivity ** [%]	Resolution [mm]	Sensitivity [%]
SPECT ^{99m} Tc	0.38–0.76 (37)	0.07–0.39 (37)	~10	~0.01
SPECT ¹¹¹ In	0.71–0.85 (37)	–	–	~0.01
Pinhole PET ¹⁸ F	<0.85* (38)	0.37 (38)	–	–
Coincidence PET ¹⁸ F	1.61–2.34 (39)	1.19–6.72 (39)	6.4 (40)	1.33–2.29 (41)
Coincidence PET ⁶⁸ Ga	2.19 (42), 2.2 (43)	–	7 (40)	–

*Resolution was determined by visual assessment of a Jaszczak phantom instead of measuring the FWHM of a line source. **Values for sensitivity should be interpreted with care, as no standard method exists to directly compare SPECT and coincidence PET sensitivity quantitatively. When covering a FOV the size of a PET FOV, the effective sensitivity of SPECT could well be several factors lower.

Green colour indicates which modality performs better in a certain area, red indicates lower performance.

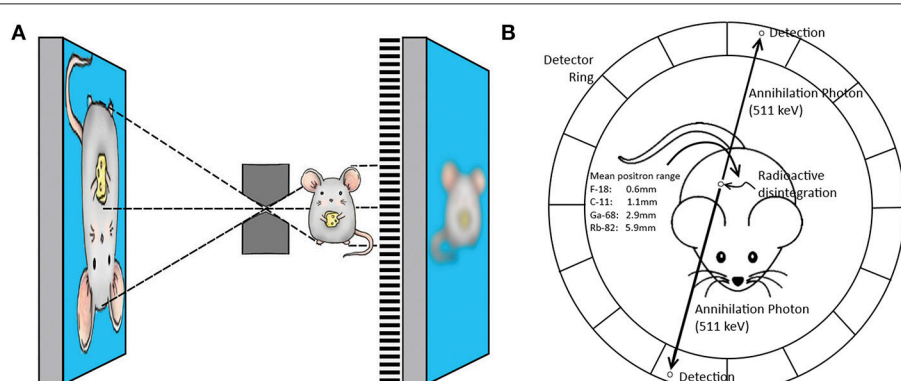


FIGURE 1 | Panel (A) illustrates the principle of pinhole imaging. The collimator can be placed close to the source of radiation in preclinical imaging, resulting in a magnifying effect on the detector. The limited sensitivity is improved by using multiple pinholes and different pinhole geometries. Clinical SPECT mostly uses parallel hole collimators, which directly limits spatial resolution. Pinhole magnification can also achieve a higher spatial resolution for positron emitting isotopes in comparison to traditional coincidence PET (Image reproduced from thesis O. Ivashchenko, LUMC, ISBN 978-94-92516-35-0). Panel (B) shows the principle of PET coincidence detection. Two opposing detectors simultaneously measure a gamma photon providing the line along which the positron annihilated with an electron. This line does not coincide with the location the positron was emitted, because the positron travels a finite range before it annihilates. Especially for high energy positrons, e.g., ⁶⁸Ga [mean positron range of 2.9 mm (46)], the positron range may limit spatial resolution in both pinhole PET and coincidence PET. Image adapted with permission from Fontaine et al. (47).

come with the obvious trade-off of lower sensitivity. Multipinhole cameras combat the very low sensitivity of a single pinhole (39), and can reduce or even eliminate the need of rotating detectors or movement of the bed if only a small field of view (FOV) is required to answer the research question (48, 49). This greatly improves temporal resolution, offers the possibility of 3D gated imaging of the heart, and enables imaging of fast tracer kinetics (50). High sensitivity collimators have been developed (51), but the sensitivity of SPECT systems remains limited in comparison to that of PET because of the relatively low fraction of photons transmitted through the collimators.

Preclinical PET

The sensitivity of PET scanners is at least an order of magnitude higher than SPECT cameras [>10 times (52), see Table 1], since no physical collimator is needed. In preclinical PET (ring diameter < 20 cm), the resolution is mostly limited by the positron range and the size of the detector elements. For low energy positron emitters (^{18}F) both factors limit spatial resolution, for high energy positron emitters (^{68}Ga) the positron range is the main limiting factor (40, 52, 53).

Positron emitting radionuclides can be imaged with a traditional coincidence based PET system and also with special pinhole collimation (54, 55). Traditional ring PET systems can achieve a better image quality in very low count rate studies, for higher count rate studies a multi-pinhole system may yield higher quality images due to the higher spatial resolution that can be achieved by pinhole magnification.

Hybrid Imaging

Use of hybrid systems, providing an anatomical reference by (contrast-enhanced) CT or MRI (1, 2, 39, 56), are crucial in atherosclerotic mouse studies because the small plaques are located close to other tissues. MRI has the major advantage of providing soft tissue contrast, which is crucial to distinguish arteries from surrounding tissue. However, the better resolution and faster scanning time of CT make this method preferable in many instances, especially if contrast agents can be used. Moreover, CT provides direct means for attenuation correction (57), whereas an MR image is usually segmented into different tissue classes to obtain an estimate of the amount of attenuating material. New opportunities are opened by the combination of more modalities, such as optical tomography, or integrating PET and SPECT to allow dual-tracer imaging. Moreover, dual tracer imaging is also explored in PET (reviewed in Walrand et al. (58), allowing further possibilities in tracer imaging.

Preclinical vs. Clinical Imaging

Preclinical SPECT can achieve a higher spatial resolution than preclinical PET platforms, whereas this is the other way round in clinical imaging (see Table 1). The higher resolution of preclinical SPECT often makes it the imaging method of choice for imaging of atherosclerotic mice because of the small sized plaques. Preclinical visualization of plaques with PET isotopes can further be complicated by positron range, as this can exceed the size of a plaque [e.g., ^{68}Ga has a mean positron range of 2.9 mm

(46)]. Image quality of clinical PET can be improved by Time of Flight (ToF), which reduces image noise by incorporating the time difference of the detected annihilation photon pair in the reconstruction. Clinical systems obtain a timing resolution of ~ 300 ps (59). In a preclinical system image quality did not improve for a timing resolution of 260 ps (60). Another difference comprises the small deviation from 180° between the annihilating photon pair (non-collinearity) that reduces the spatial resolution for systems with a larger PET ring diameter. This becomes a major limiting factor in clinical PET (52), whilst this effect is negligible in small animal PET. Also, in clinical practice gated imaging is used to improve image quality of moving structures like the heart and its coronary arteries (61, 62). A trade-off has to be made between scan time and image quality to obtain sufficient count statistics in each gate. Using image registration techniques, motion-free static images can be obtained without affecting count statistics (63). This application is thus far not commonly applied in preclinical imaging. Finally, the high sensitivity and simultaneous acquisition of all projection angles in whole body PET makes it superior over SPECT with regard to temporal resolution, as the time needed to obtain sufficient counts directly determines scanning time.

Image Reconstruction

Virtually all preclinical and clinical images are reconstructed by an iterative reconstruction algorithm. These algorithms rely on a model of the physics in the imaging process, where improvement of the model improves the quality of the reconstructed images. For example, spatial resolution can be improved by including the point spread function in the model (64). Monte Carlo based methods can improve scatter estimation and can include depth of interaction effects for PET in the iterative reconstruction (65, 66). Efficient algorithms can reduce reconstruction time while preserving image quality even in low count studies (67).

Quantification

Besides visualizing the radiotracer distribution, most atherosclerosis imaging studies perform (semi-) quantitative Volume Of Interest (VOI) or voxel based measurements. This is expressed in percentage injected dose per gram, standardized uptake value, or target to background ratio (%ID/g, SUV, or TBR). It is important to consider against which background a target tissue is visualized. Plaque to blood ratio is usually a useful TBR in atherosclerosis imaging, as blood signal can interfere with plaque signal. The myocardium would be a suitable background when using a radiotracer such as $[^{18}\text{F}]$ FDG in the coronary arteries. Images can be quantified when applying a suitable predetermined calibration factor to convert counts per volume to activity per volume (Bq/ml). Attenuation and scatter correction is less important in preclinical imaging due to the smaller amount of attenuating material, but their application still improves quantification accuracy (57, 68–70). When imaging structures with sizes around or below the resolution of the camera, like plaques in mice, it is important to realize that partial volume effects can cause a substantial underestimation of the true value (71, 72). This makes absolute quantification accuracy dependent

TABLE 2 | Shows radiotracers applied in a selection of preclinical *in vivo* atherosclerosis imaging studies from 2008 to 2018, and mentions potential clinical follow-up studies.

Disease characteristic	Target	Ligand	Radionuclide	Animal studies	Clinical studies
Inflammation	Macrophages	FDG	¹⁸ F	(13)	(11) retrospective, <i>n</i> = 513
	Macrophages, SST2	DOTATATE	⁶⁸ Ga	(75)	(76) retrospective, <i>n</i> = 70 (77) Prospective, <i>n</i> = 20 (78) Prospective, <i>n</i> = 42
	Macrophages, MR	FDM	¹⁸ F	(79)	
		Tilmanocept	¹¹¹ In	(80)	
	Macrophages, FR	EC20	^{99m} Tc	(81)	
		ECO800	¹¹¹ In	(82)	
		FOL	¹⁸ F	(83)	
	Macrophages, CXCR4	Pentixafor	⁶⁸ Ga	(84)	(85) Retrospective, <i>n</i> = 38 (86) Retrospective, <i>n</i> = 51
	Leukocytes, LFA-1	DANBIRT	¹¹¹ In	(87)	
	Macrophage proliferation	FLT	¹⁸ F	(88)	
Apoptosis	Chemokine receptors	DOTA-vMIP-II	⁶⁴ Cu	(89, 90)	
		DOTA-DAPTA	⁶⁴ Cu	(91)	
	LOX-1	Liposome-LOX-1	¹¹¹ In	(92)	
		Camelid antibody fragment	^{99m} Tc	(93)	
	TSPO	PK11195	¹¹ C		(94)
		Ge-180	¹⁸ F		Prospective, <i>n</i> = 15 (95) Prospective, <i>n</i> = 32 (96)
	Macrophage phagocytosis	TNP	⁶⁴ Cu		
		Macroflor	¹⁸ F	(97)	
	Apoptosis and Necrosis	AnxAF568	^{99m} Tc,	(99)	
		Hypericin	¹²⁴ I		
Angiogenesis	Apoptosis	Duramycin	^{99m} Tc	(100)	
	Apoptosis	Duramycin and Annexin V	^{99m} Tc	(101)	
	$\alpha_v\beta_3$ integrin	NC100692	^{99m} Tc	(102)	
		NOTA-RGD	⁶⁸ Ga	(103)	(103) Prospective, <i>n</i> = 4
		Flotegatide	¹⁸ F	(104)	
		Galacto-RGD	¹⁸ F	(105)	(106) Prospective, <i>n</i> = 10
		NOTA-3-4A	⁶⁴ Cu	(107)	
		Maracilatide	^{99m} Tc	(108)	
		IDA-D-[c(RGDfK)] ₂	^{99m} Tc	(109)	
	VEGF 1 and 2	scV/Tc	^{99m} Tc	(110, 111)	
Proteolysis	MMP activation	RP805	^{99m} Tc	(112, 113)	
		RP782	¹¹¹ In	(114, 115)	
	GPVI	GPVI-fragment crystallized	⁶⁴ Cu	(116)	
	P-selectin	P-selectin antibody	⁶⁴ Cu	(117)	
		Fucoidan	⁶⁸ Ga	(118)	
Endothelial activation	VCAM-1	cAbVCAM1-5	^{99m} Tc	(119–121)	
			¹⁸ F	(122)	
		4V	¹⁸ F	(123)	
		FMISO	¹⁸ F	(124)	
Hypoxia	Redox				

SST2, somatostatin receptor subtype 2; MR, Mannose Receptor; FR, Folate Receptor; CXCR4, C-X-C Chemokine Receptor type 4; LFA-1, Leukocyte Function associated Antigen-1; LOX-1, oxidized LDL receptor 1; TSPO, Translocatio Protein; VEGF, Vascular Endothelial Growth Factor; MMP, Matrix Metalloprotease; GPVI, Platelet Glycoprotein VI; VCAM-1, Vascular Cell Adhesion Molecule-1.

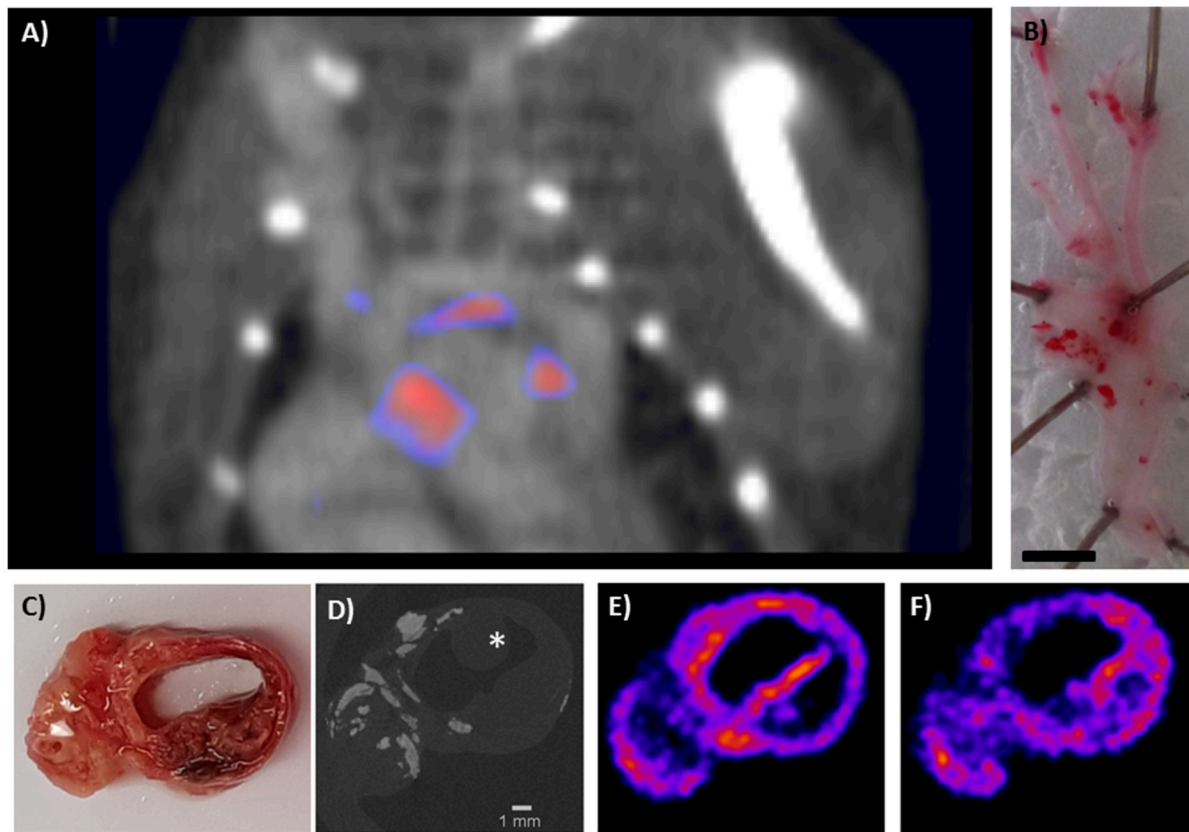


FIGURE 2 | Two cases which exemplify the opportunities and challenges in preclinical imaging using multi-pinhole collimators. Panel (A) shows a contrast enhanced SPECT/CT scan of the thoracic region of an ApoE^{-/-} mouse (on 20 weeks high fat diet), imaged with [¹¹¹In]In-DANBIRT, which targets leukocytes via Leukocyte Function associated Antigen 1 (LFA-1). LFA-1 is expressed in a high-affinity state on leukocytes near regions of inflammation, and can therefore be used to visualize inflamed plaque. The image shows uptake in plaque regions in the inner curve of the aortic arch and near the aortic leaflets. These common sites of plaque formation in this mouse model are visible in the excised, opened Oil Red O stained artery of an ApoE^{-/-} mouse on the right (B). Panel (A) shows the high resolution which can be achieved with preclinical SPECT, considering the mouse aorta is ~1 mm in diameter. This case also illustrates some of the challenges in preclinical imaging as the small size of the plaque and the presence of few target cells require a state of the art imaging system with high resolution and sensitivity. Moreover, the recommended injection dose of 20 µL contrast agent per 5 g bodyweight (Exitron nano 12000) can be challenging, as the combined injection volume of contrast agent and radiotracer injection can easily exceed the recommended injection volume for mice, which can have adverse effects on the animal health and experimental outcome. Reduction of the injection volume of the radiopharmaceuticals can be achieved by using smaller tubing during radiolabelling. The timing of injection is also important, as blood signal of radiotracers can be high after injection, yet the amount of activity reduces with radionuclide half-life. Moreover, many contrast agents circulate a limited period in the vasculature. Optimization before an experiment, considering the dose and timing of injection, is therefore crucial. In this example, we injected 50 MBq (200 pmol) [¹¹¹In]In-DANBIRT 2 h before SPECT imaging, and the contrast agent directly at the start of CT imaging. Scale bar = 2 mm [reproduced from Meester et al. (87), no permissions required]. (C–F) depict an example of a high resolution dual-isotope preclinical SPECT/CT scanning protocol applied to diseased human arterial tissue. Examination of the local differences in dual-radiotracer uptake with respect to the atherosclerotic pathophysiology was performed on (C) a human carotid endarterectomy slice of 2 mm thickness, which was incubated for 60 min with [¹¹¹In]In-DANBIRT (targeting leukocytes) and [^{99m}Tc]Tc-DEMOTATE (targeting activated macrophages; both 1 nmol, 100 MBq/nmol). [^{99m}Tc]Tc-DEMOTATE targets somatostatin receptor subtype 2, which is expressed on activated macrophages. (D) Functional plaque morphology was resolved with high resolution µCT (15 min scan, full scan angle, 0.24 mA, 50 kV, 75 ms, 500 µm reconstructed resolution), where calcifications are denoted by the bright white regions. The asterisk (*) marks the sample holder. µCT was co-registered to SPECT (90 min scan) reconstructions of (E) [¹¹¹In]In-DANBIRT and (F) [^{99m}Tc]Tc-DEMOTATE. The two radioisotopes can be separated by selecting the correct energy windows for the photon peaks of ¹¹¹In and ^{99m}Tc (¹¹¹In photopeaks 171 and 245 keV, energy windows 158–187 keV and 219–267 keV, ^{99m}Tc photopeak 140 keV, energy window 125–152 keV). This hybrid functional imaging approach can be used to gain greater insights into radiotracer uptake in diseased tissues. Plaque status can be assessed via the presence of calcifications, whereas [¹¹¹In]In-DANBIRT and [^{99m}Tc]Tc-DEMOTATE ascertain inflammatory status by visualizing total inflammation and activated macrophages, respectively. Such scans could lead to a better risk stratification of atherosclerotic patients. It is interesting to see the different distribution patterns of these inflammation-targeted tracers within the plaque, which indicates that plaque detection alone gives only limited information when making a risk stratification of atherosclerotic patients. The timing of imaging is important as the radionuclides have different half-lives, and correct separation of the photon peaks requires sufficient counts to be acquired. Another challenge is to examine which incubation time allows the radiotracers to diffuse into the tissue, while keeping tissue degradation at a minimum (Courtesy H.E.B, Erasmus MC).

on the imaging task. Numerous compensation techniques for partial volume effects have been described (73), but none have been validated or used in preclinical atherosclerosis imaging yet.

RADIOTRACERS AND THEIR TARGETS

Radiotracers and Radionuclides

Radiotracers should target processes relevant to disease, which in atherosclerosis are e.g., inflammation, endothelial dysfunction, neovascularization, hypoxia, cell death, or microcalcification. Moreover, the target should ideally be abundantly expressed and specifically localized in plaques and not in surrounding tissues. Also, blocking studies should be performed, as non-specific uptake in the arterial wall could complicate plaque visualization. Radiotracers need to be stable *in vivo* without pharmacological or toxic effects, and should be labeled with an appropriate radionuclide, matching the pharmacokinetics of the tracer. Radiotracers labeled with short-lived PET radionuclides should have a fast clearance to prevent blood signal from interfering with plaque visualization. Moreover, it is advantageous if radiotracers show rapid diffusion into tissues. If a radiopharmaceutical is being developed with the objective of use in humans, then the radionuclide intended for human use should be used in the animal studies if at all possible as this will simplify translation of preclinical data. In some cases, however, the use of a different radionuclide for some of the preclinical studies is unavoidable or even preferable, as it can be preferred to label radiotracers with SPECT radionuclides for high-resolution preclinical evaluation vs. PET radionuclides for clinical use.

Beyond [¹⁸F]FDG

[¹⁸F]FDG PET has shown major promise in atherosclerosis imaging (8). [¹⁸F]FDG, being a glucose analog, is taken up by metabolically active cells such as macrophages in plaque, and can therefore be used for PET imaging of atherosclerosis. Plaque inflammation can be quantified using [¹⁸F]FDG, plaques can be monitored over time, and the effect of treatment can be visualized (74). However, unspecific myocardial uptake of [¹⁸F]FDG limits the applicability of imaging in coronary artery disease. Therefore, novel radiotracers targeting different disease processes with a higher specificity are being developed and evaluated. **Table 2** lists a number of radiotracers and their targets tested in preclinical *in vivo* imaging studies in the past 10 years, and potential clinical follow up studies. **Figure 2** includes 2 cases in which the possibilities and challenges of small radionuclide imaging of atherosclerosis are exemplified. Reference (125) reviews older studies performed with PET.

Currently, [⁶⁸Ga]Ga-Pentixafor (84, 85), [⁶⁸Ga]Ga-DOTATATE (75, 78), and [¹⁸Na]NaF (reviewed in Mckenney-drake et al. 9) show very promising results in patients. Recent successful mouse studies have been performed on other tracers such as [¹¹¹In]In-DANBIRT (87), [¹¹¹In]In-Tilmanocept (80), or [^{99m}Tc]Tc-Maracilatide (108). Direct comparisons between radiotracers as performed in Rinne et al. (75), are lacking however, which makes it difficult to see where radiotracers can complement each other, or which radiotracer is most suitable for different aspects of plaque visualization.

PERSPECTIVES AND RECOMMENDATIONS

Risk Stratification in Atherosclerosis

The development of non-invasive imaging techniques visualizing atherosclerosis and particularly vulnerable plaque is a major aim in cardiovascular imaging (126). The individual and societal impact of such imaging tools can be substantial. They could contribute to current risk stratification, which is based on conventional cardiovascular risk factors and non-traditional risk factors such as biomarkers and coronary artery calcium score. Recent clinical trials focus on the importance of anti-inflammatory strategies for treatment of cardiovascular disease (127, 128). Biomarkers (e.g., hsCRP, IL-6) are mostly used for assessment of inflammation, and might be complemented by non-invasive molecular imaging of arterial inflammation in guiding treatment with these new anti-inflammatory drugs. Novel tracers therefore could provide extra prognostic value, and aid in further risk-stratification by identifying plaques at risk and patients in need of treatment.

Crossing Borders

Diagnostic imaging tools developed for other (non-cardiac) diseases such as oncology have been shown to be of significance in atherosclerosis research (129). Somatostatin receptor imaging using ⁶⁸Ga-DOTATATE, developed for diagnosis of neuro-endocrine tumors, has been validated as a novel marker of atherosclerotic inflammation via overexpression of the somatostatin receptor subtype 2 (SST2) on activated macrophages. This has led to better discriminating power of high risk coronary lesions compared to [¹⁸F]FDG (75, 78). Similarly, imaging of macrophages with ⁶⁸Ga-Pentixafor also originates from oncology (84, 85). Furthermore, technical challenges in image post-processing in atherosclerosis might be improved by developments from other research fields (130, 131). Vice versa, research on other diseases can benefit from our increased knowledge, as diagnosis of other inflammatory diseases such as arthritis can be difficult and hampered by similar challenges encountered in atherosclerosis.

CONCLUSION

Developments in animal models and imaging systems have facilitated and enhanced the opportunities for small radionuclide imaging and will likely continue to do so in the foreseeable future. These advances have been essential in preclinical imaging of atherosclerosis, which requires high resolution and sensitivity, and has resulted in a large number of novel radiotracers being evaluated. This allows ample opportunity for clinical translation, where more insight into atherosclerosis, as well as relevant imaging targets, are highly required.

DATA AVAILABILITY

The datasets generated for this study are available on request to the corresponding author.

AUTHOR CONTRIBUTIONS

All authors listed have made a substantial, direct and intellectual contribution to the work, and approved it for publication.

REFERENCES

1. Wehr HF, Wiehr S, Divine MR, Gatzidis S, Gullberg GT, Maier FC, et al. Preclinical and translational PET/MR imaging. *J Nucl Med.* (2014) 55:11S–8S. doi: 10.2967/jnumed.113.129221
2. Gaitanis A, Kastis GA, Vlastou E, Bouziotis P, Verginis P, Anagnostopoulos CD. Investigation of image reconstruction parameters of the mediso nanoscan PC small-animal PET/CT scanner for two different positron emitters under NEMA NU 4-2008 standards. *Mol Imaging Biol.* (2017) 19:550–9. doi: 10.1007/s11307-016-1035-9
3. Lauber DT, Fülop A, Kovács T, Szegedi K, Máthé D, Szijártó A. State of the art *in vivo* imaging techniques for laboratory animals. *Lab Anim.* (2017) 1:14. doi: 10.1177/0023677217695852
4. España S, Marcinkowski R, Keereman V, Vandenberghe S, van Holen R. DigiPET : sub-millimeter spatial resolution small-animal PET imaging using thin monolithic scintillators. *Phys Med Biol.* (2014) 59:13. doi: 10.1088/0031-9155/59/13/3405
5. Nekolla SG, Rischpler C, Paschali A, Anagnostopoulos C. Cardiovascular preclinical imaging. *Q J Nucl Med Mol Imaging.* (2017) 61:48–59. doi: 10.23736/S1824-4785.16.02960-5
6. Ivashchenko O, Have F Van Der, Goorden MC, Ramakers RM, Beekman FJ. Ultra-high-sensitivity submillimeter mouse SPECT. *J Nucl Med.* (2015) 56:470–6. doi: 10.2967/jnumed.114.147140
7. Virmani R, Kolodgie FD, Burke AP, Farb A, Schwartz SM. Lessons from sudden coronary death a comprehensive morphological classification scheme for atherosclerotic lesions. *Arter Thromb Biol.* (2000) 20:1262–75. doi: 10.1161/01.ATV.20.5.1262
8. Rudd JHF, Warburton EA, Fryer TD, Jones HA, Clark JC, Antoun N, et al. Imaging atherosclerotic plaque inflammation with [18F]-fluorodeoxyglucose positron emission tomography. *Circulation.* (2002) 105:2708–11. doi: 10.1161/01.CIR.0000020548.60110.76
9. Mckenney-drake ML, Moghbel MC, Paydary K, Alloosh M, Houshmand S, Höilund-carlsén PF, et al. 18 F-NaF and 18 F-FDG as molecular probes in the evaluation of atherosclerosis. *Eur J Nucl Med Mol Imaging.* (2018) 2190–200. doi: 10.1007/s00259-018-4078-0
10. Marnane M, Merwick A, Sheehan OC, Hannon N, Foran P, Grant T, et al. Carotid plaque inflammation on 18F-fluorodeoxyglucose positron emission tomography predicts early stroke recurrence. *Ann Neurol.* (2012) 71:709–18. doi: 10.1002/ana.23553
11. Figueroa AL, Abdelbaky A, Truong QA, Corsini E, MacNabb MH, Lavender ZR, et al. Measurement of arterial activity on routine FDG PET/CT images improves prediction of risk of future CV events. *JACC Cardiovasc Imaging.* (2013) 6:1250–9. doi: 10.1016/j.jcmg.2013.08.006
12. Moon SH, Cho YS, Noh TS, Choi JY, Kim BT, Lee KH. Carotid FDG uptake improves prediction of future cardiovascular events in asymptomatic individuals. *JACC Cardiovasc Imaging.* (2015) 8:949–56. doi: 10.1016/j.jcmg.2015.06.002
13. Wenning C, Kloth C, Kuhlmann MT, Jacobs AH, Schober O, Hermann S, et al. Serial F-18-FDG PET/CT distinguishes in flamed from stable plaque phenotypes in shear-stress induced murine atherosclerosis. *Atherosclerosis.* (2014) 234:276–82. doi: 10.1016/j.atherosclerosis.2014.03.008
14. Getz GS, Reardon CA. Animal models of atherosclerosis animal models of atherosclerosis. *Arterioscler Thromb Vasc Biol.* (2012) 32:1104–15. doi: 10.1161/ATVBAHA.111.237693
15. Fan J, Kitajima S, Watanabe T, Xu J, Zhang J, Liu E, et al. Rabbit models for the study of human atherosclerosis: from pathophysiological mechanisms to translational medicine. *Pharmacol Ther.* (2015) 2015:104–19. doi: 10.1016/j.pharmthera.2014.09.009
16. Jarrett KE, Lee C, De Giorgi M, Hurley A, Gillard BK, Doerfler AM, et al. Somatic Editing of *Ldlr* with adeno-associated viral-CRISPR is an efficient tool for atherosclerosis research. *Arterioscler Thromb Vasc Biol.* (2018) 28:1997–2006. doi: 10.1161/ATVBAHA.118.311221
17. Kumar S, Kang DW, Rezvan A, Jo H. Accelerated atherosclerosis development in C57Bl6 mice by overexpressing AAV-mediated PCSK9 and partial carotid ligation. *Lab Investig.* (2017) 97:935–45. doi: 10.1038/labinvest.2017.47
18. Veseli BE, Perrotta P, De Meyer GRA, Roth L, Van der Donck C, Martinet W, et al. Animal models of atherosclerosis. *Eur J Pharmacol.* (2017) 816:3–13. doi: 10.1016/j.ejphar.2017.05.010
19. Suo J, Ferrara DE, Sorescu D, Guldberg RE, Taylor WR, Giddens DP. Hemodynamic shear stresses in mouse aortas: implications for atherogenesis. *Arterioscler Thromb Vasc Biol.* (2007) 27:346–51. doi: 10.1161/01.ATV.0000253492.45717.46
20. Li X, Liu Y, Zhang H, Ren L, Li Q, Li N. Animal models for the atherosclerosis research: a review. *Protein Cell.* (2011) 2:189–201. doi: 10.1007/s13238-011-1016-3
21. Falk E. Pathogenesis of atherosclerosis. *J Am Coll Cardiol.* (2006) 47:C7–12. doi: 10.1016/j.jacc.2005.09.068
22. Daechin V, Sluimer JC, van der Heiden K, Skachkov I, Kooiman K, Janssen A, et al. Live observation of atherosclerotic plaque disruption in apolipoprotein E-deficient mouse. *Ultrasound Int Open.* (2015) 01:E67–71. doi: 10.1055/s-0035-1565092
23. Zhang S, Picard MH, Vasile E, Zhu Y, Raffai RL, Weisgraber KH, et al. Diet-induced occlusive coronary atherosclerosis, myocardial infarction, cardiac dysfunction, and premature death in scavenger receptor class B type I-deficient, hypomorphic apolipoprotein ER61 mice. *Circulation.* (2005) 111:3457–64. doi: 10.1161/CIRCULATIONAHA.104.523563
24. Van Herck JL, De Meyer GRY, Martinet W, Van Hove CE, Foubert K, Theunis MH, et al. Impaired fibrillin-1 function promotes features of plaque instability in apolipoprotein E-deficient mice. *Circulation.* (2009) 120:2478–87. doi: 10.1161/CIRCULATIONAHA.109.872663
25. Heiden K Van Der, Hoogendoorn A, Daemen MJ, Gijssen FJH. Animal models for plaque rupture : a biomechanical assessment. *Thromb Haemost.* (2016) 115:501–8. doi: 10.1160/TH15-07-0614
26. Mestas J, Hughes CCW. Of mice and not men: differences between mouse and human immunology. *J Immunol.* (2004) 172:2731–8. doi: 10.4049/jimmunol.172.5.2731
27. Martinez FO, Helming L, Milde R, Varin A, Melgert BN, Draijer C, et al. Genetic programs expressed in resting and IL-4 alternatively activated mouse and human macrophages: similarities and differences. *Blood.* (2013) 121:57–70. doi: 10.1182/blood-2012-06-436212
28. Jager NA, Westra J, Golestan R, van Dam GM, Low PS, Tio RA, et al. Folate receptor-β imaging using 99mTc-folate to explore distribution of polarized macrophage populations in human atherosclerotic plaque. *J Nucl Med.* (2014) 55:1945–51. doi: 10.2967/jnumed.114.143180
29. Irkle A, Vesey AT, Lewis DY, Skepper JN, Bird JLE, Dweck MR, et al. Identifying active vascular microcalcification by 18F-sodium fluoride positron emission tomography. *Nat Commun.* (2015) 6:7495. doi: 10.1038/ncomms8495
30. de Kemp RA, Epstein FH, Catana C, Tsui BMW, Ritman EL. Small-animal molecular imaging methods. *J Nucl Med.* (2010) 51:18S–32S. doi: 10.2967/jnumed.109.068148
31. Van Audenhaege K, Van Holen R, Vandenberghe S, Vanhove C, Metzler SD, Moore SC. Review of SPECT collimator selection, optimization, and fabrication for clinical and preclinical imaging. *Med Phys.* (2015) 42:4796–813. doi: 10.1118/1.4927061

FUNDING

This work was supported by a grant from the Erasmus MC. KvdH is funded by the Netherlands Heart Foundation (Proj. no. NHS2014T096).

32. Yao R, Lecomte R, Crawford ES. Small-animal PET: what is it, and why do we need it? *J Nucl Med Technol.* (2012) 40:157–65. doi: 10.2967/jnmt.111.098632
33. Wells RG. Instrumentation in molecular imaging. *J Nucl Cardiol.* (2016) 6:1343–7. doi: 10.1007/s12350-016-0498-z
34. Clark DP, Badea CT. Micro-CT of rodents: state-of-the-art and future perspectives. *Phys Med.* (2014) 30:619–34. doi: 10.1016/j.ejmp.2014.05.011
35. Weissleder R, Ross BD, Rehemtulla A, Gabmhir SS. *Molecular Imaging: Principles and Practice.* Shelton, CT: PMPH (2011).
36. Zaidi H. Molecular imaging of small animals: instrumentation and applications. New York, NY: Springer-Verlag (2014).
37. Deleye S, Van Holen R, Verhaeghe J, Vandenberghe S, Stroobants S, Staelens S. Performance evaluation of small-animal multipinhole μ sPECT scanners for mouse imaging. *Eur J Nucl Med Mol Imaging.* (2013) 40:744–58. doi: 10.1007/s00259-012-2326-2
38. Walker MD, Goorden MC, Dinelle K, Ramakers RM, Blinder S, Shirmohammad M, et al. Performance assessment of a preclinical PET scanner with pinhole collimation by comparison to a coincidence-based small-animal PET scanner. *J Nucl Med.* (2014) 55:1368–74. doi: 10.2967/jnmed.113.136663
39. Goertzen AL, Bao Q, Bergeron M, Blankemeyer E, Blinder S, Cañadas M, et al. Comparison of preclinical PET imaging systems. *J Nucl Med.* (2012) 53:1300–9. doi: 10.2967/jnmed.111.099382
40. Sanchez-Crespo A. Comparison of Gallium-68 and Fluorine-18 imaging characteristics in positron emission tomography. *Appl Radiat Isot.* (2013) 76:55–62. doi: 10.1016/j.apradiso.2012.06.034
41. Ilan E, Deller T, Kjellberg F, Peterson W, Lubberink M. Performance comparison of three commercially available PET systems: SIGNA PET/MR, discovery IQ and discovery MI. *J Nucl Med.* (2017) 58(Suppl 1):1353.
42. Liu X, Laforest R. Quantitative small animal PET imaging with nonconventional nuclides. *Nucl Med Biol.* (2009) 36:551–9. doi: 10.1016/j.nucmedbio.2009.01.019
43. Canadas M, Sanz ER, Vives MO, Vaquero JJ, Desco M, Vicente E, et al. Performance evaluation for ^{68}Ga and ^{18}F of the ARGUS small-animal PET scanner based on the NEMA NU-4 standard. In: *IEEE Nuclear Science Symposium & Medical Imaging Conference.* Knoxville, TN: IEEE (2010). p. 3454–7. doi: 10.1109/NSSMIC.2010.5874448
44. Anger HO. Scintillation camera with multichannel collimators. *J Nucl Med.* (1964) 5:515–31.
45. Beekman F, van Der Have F. The pinhole: gateway to ultra-high-resolution three-dimensional radionuclide imaging. *Eur J Nucl Med Mol Imaging.* (2007) 34:151–61. doi: 10.1007/s00259-006-0248-6
46. Partridge M, Spinelli A, Ryder W, Hindorf C. The effect of $\beta+$ -energy on performance of a small animal PET camera. *Nucl Inst Methods Phys Res.* (2006) 568:933–6. doi: 10.1016/j.nima.2006.09.035
47. Fontaine R, Bélanger F, Cadorette J, Leroux JD, Martin JP, Michaud JB, et al. Architecture of a dual-modality, high-resolution, fully digital positron emission tomography/computed tomography (PET/CT) scanner for small animal imaging. *IEEE Trans Nucl Sci.* (2005) 52:691–6. doi: 10.1109/TNS.2005.850484
48. Branderhorst W, Vastenhout B, Van Der Have F, Blezer ELA, Bleeker WK, Beekman FJ. Targeted multi-pinhole SPECT. *Eur J Nucl Med Mol Imaging.* (2011) 38:552–61. doi: 10.1007/s00259-010-1637-4
49. Lange C, Apostolova I, Lukas M, Huang KP, Hofheinz F, Gregor-Mamoudou B, et al. Performance evaluation of stationary and semi-stationary acquisition with a non-stationary small animal multi-pinhole SPECT system. *Mol Imaging Biol.* (2014) 16:311–6. doi: 10.1007/s11307-013-0702-3
50. Vaissier PEB, Goorden MC, Vastenhout B, van der Have F, Ramakers RM, Beekman FJ. Fast spiral SPECT with stationary -cameras and focusing pinholes. *J Nucl Med.* (2012) 53:1292–9. doi: 10.2967/jnmed.111.101899
51. Mahani H, Raisali G, Kamali-Asl A, Ay MR. Spinning slit-hole collimation for high-sensitivity small animal SPECT: design and assessment using GATE simulation. *Phys Med.* (2017) 40:42–50. doi: 10.1016/j.ejmp.2017.07.005
52. Rahmim A, Zaidi H. PET versus SPECT: strengths, limitations and challenges. *Nucl Med Commun.* (2008) 29:193–207. doi: 10.1097/MNM.0b013e3282f3a515
53. Levin CS, Hoffman EJ. Calculation of positron range and its effect on the fundamental limit of positron emission tomography system spatial resolution. *Phys Med Biol.* (1999) 44:781–99. doi: 10.1088/0031-9155/44/3/019
54. Goorden MC, van der Have F, Kreuger R, Ramakers RM, Vastenhout B, Burbach JPH, et al. VECToR: a preclinical imaging system for simultaneous submillimeter SPECT and PET. *J Nucl Med.* (2013) 54:306–12. doi: 10.2967/jnmed.112.109538
55. DiFilippo FP. Design of a Tri-PET collimator for high-resolution whole-body mouse imaging. *Med Phys.* (2017) 44:4230–8. doi: 10.1002/mp.12379
56. Hamamura MJ, Ha S, Roeck WW, Wagenaar DJ, Meier D, Patt BE, et al. Initial investigation of preclinical integrated SPECT and MR imaging. *Technol Cancer Res Treat.* (2010) 9:21–7. doi: 10.1177/15330346100090103
57. Vanhove C, Defrise M, Bossuyt A, Lahoutte T. Improved quantification in multiple-pinhole SPECT by anatomy-based reconstruction using microCT information. *Eur J Nucl Med Mol Imaging.* (2009) 38:153–65. doi: 10.1007/s00259-010-1627-6
58. Walrand S, Hesse M, Jamar F. Update on novel trends in PET / CT technology and its clinical applications. *Br J Radiol.* (2018) 218:89. doi: 10.1259/bjr.20160534
59. Surti S, Karp JS. Advances in time-of-flight PET. *Phys Med.* (2016) 32:12–22. doi: 10.1016/j.ejmp.2015.12.007
60. Schug D, Lerche C, Weissler B, Gebhardt P, Goldschmidt B, Wehner J, et al. Initial PET performance evaluation of a preclinical insert for PET/MRI with digital SiPM technology. *Phys Med Biol.* (2016) 61:2851–78. doi: 10.1088/0031-9155/61/7/2851
61. Buther F, Dawood M, Stegger L, Wubbeling F, Schaefers M, Schober O, et al. List mode-driven cardiac and respiratory gating in PET. *J Nucl Med.* (2009) 50:674–81. doi: 10.2967/jnmed.108.059204
62. Rubeaux M, Joshi NV, Dweck MR, Fletcher A, Motwani M, Thomson LE, et al. Motion correction of ^{18}F -NaF PET for imaging coronary atherosclerotic plaques. *J Nucl Med.* (2016) 57:54–9. doi: 10.2967/jnmed.115.162990
63. Wu C, Vaissier PE, Vastenhout B, de Jong JR, Slart RH, Beekman FJ. Influence of respiratory gating, image filtering, and animal positioning on high-resolution electrocardiography-gated murine cardiac single-photon emission computed tomography. *Mol Imaging.* (2014) 13:1–11. doi: 10.2310/7290.2014.00052
64. Peterson TE, Shokouhi S. Advances in preclinical SPECT instrumentation. *J Nucl Med.* (2012) 53:841–4. doi: 10.2967/jnmed.111.099853
65. Magdics M, Szirmay-Kalos L, Toth B, Legrady D, Cserkaszky A, Balkay L, et al. Performance evaluation of scatter modeling of the GPU-based “Tera-Tomo” 3D PET reconstruction. In: *IEEE Nuclear Science Symposium Conference Record.* Valencia: IEEE (2011). p. 4086–8.
66. Nagy K, Toth M, Major P, Patay G, Egri G, Haggkvist J, et al. Performance evaluation of the small-animal nanoscan PET/MRI system. *J Nucl Med.* (2013) 54:1825–32. doi: 10.2967/jnmed.112.119065
67. Vaissier PEB, Beekman FJ, Goorden MC. Similarity-regulation of OS-EM for accelerated SPECT reconstruction. *Phys Med Biol.* (2016) 61:4300–15. doi: 10.1088/0031-9155/61/11/4300
68. Chen CL, Wang Y, Lee JJS, Tsui BMW. Toward quantitative small animal pinhole SPECT: assessment of quantitation accuracy prior to image compensations. *Mol Imaging Biol.* (2009) 11:195–203. doi: 10.1007/s11307-008-0181-0
69. Wu C, de Jong JR, Gratama van Andel HA, van der Have F, Vastenhout B, Laverman P, et al. Quantitative multi-pinhole small-animal SPECT: uniform versus non-uniform Chang attenuation correction. *Phys Med Biol.* (2011) 56:N183–93. doi: 10.1088/0031-9155/56/18/N01
70. Vandeghinste B, Van Holen R, Vanhove C, De Vos F, Vandenberghe S, Staelens S. Use of a ray-based reconstruction algorithm to accurately quantify preclinical microspect images. *Mol Imaging.* (2014) 13:1–13. doi: 10.2310/7290.2014.00007
71. Bettinardi V, Castiglioni I, De Bernardi E, Igliardi MC. PET quantification: strategies for partial volume correction. *Clin Transl Imaging.* (2014) 2:199–218. doi: 10.1007/s40336-014-0066-y
72. Mannheim JG, Judenhofer MS, Schmid A, Tillmanns J, Stiller D, Sossi V, et al. Quantification accuracy and partial volume effect in dependence of the

- attenuation correction of a state-of-the-art small animal PET scanner. *Phys Med Biol.* (2012) 57:3981–93. doi: 10.1088/0031-9155/57/12/3981
73. Erlandsson K, Buvat I, Pretorius PH, Thomas BA, Hutton BF. A review of partial volume correction techniques for emission tomography and their applications in neurology, cardiology and oncology. *Phys Med Biol.* (2012) 57:21. doi: 10.1088/0031-9155/57/21/R119
 74. Tawakol A, Fayad ZA, Mogg R, Alon A, Klimas MT, Dansky H, et al. Intensification of statin therapy results in a rapid reduction in atherosclerotic inflammation: results of a multicenter fluorodeoxyglucose-positron emission tomography/computed tomography feasibility study. *J Am Coll Cardiol.* (2013) 62:909–17. doi: 10.1016/j.jacc.2013.04.066
 75. Rinne P, Hellberg S, Kiugel M, Virta J, Li X-G, Käkelä M, et al. Comparison of somatostatin receptor 2-targeting PET tracers in the detection of mouse atherosclerotic plaques. *Mol Imaging Biol.* (2015) 18:99–108. doi: 10.1007/s11307-015-0873-1
 76. Rominger A, Saam T, Vogl E, Ubleis C, la Fougère C, Förster S, et al. *In vivo* imaging of macrophage activity in the coronary arteries using 68Ga-DOTATATE PET/CT: correlation with coronary calcium burden and risk factors. *J Nucl Med.* (2010) 51:193–7. doi: 10.2967/jnumed.109.070672
 77. Wan MYS, Endozo R, Michopoulos S, Shortman R, Rodriguez-Justo M, Menezes L, et al. PET/CT imaging of unstable carotid plaque with Ga-68 labelled somatostatin receptor ligand. *J Nucl Med.* (2017) 58:774–80. doi: 10.2967/jnumed.116.181438
 78. Tarkin JM, Joshi FR, Evans NR, Chowdhury MM, Figg NL, Shah AV, et al. Detection of atherosclerotic inflammation by 68Ga-DOTATATE PET compared to [18F]FDG PET imaging. *J Am Coll Cardiol.* (2017) 69:1774–91. doi: 10.1016/j.jacc.2017.01.060
 79. Tahara N, Mukherjee J, de Haas HJ, Petrov AD, Tawakol A, Haider N, et al. 2-deoxy-2-[18F]fluoro-D-mannose positron emission tomography imaging in atherosclerosis. *Nat Med.* (2014) 20:215–9. doi: 10.1038/nm.3437
 80. Varasteh Z, Hyafil F, Anizan N, Diallo D, Aid-launais R, Mohanta S, et al. Targeting mannose receptor expression on macrophages in atherosclerotic plaques of apolipoprotein E-knockout mice using In-tilmanocept. *EJNMMI Res.* (2017) 7:40. doi: 10.1186/s13550-017-0287-y
 81. Ayala-lopez W, Xia W, Varghese B, Low PS. Imaging of atherosclerosis in apolipoprotein E knockout mice : targeting of a folate-conjugated radiopharmaceutical to activated macrophages. *J Nucl Med.* (2010) 51:768–74. doi: 10.2967/jnumed.109.071324
 82. Winkel LCJ, Groen HC, van Thiel BS, Müller C, van der Steen AFW, Wentzel JJ, et al. Folate receptor-targeted single-photon emission computed tomography/computed tomography to detect activated macrophages in atherosclerosis: can it distinguish vulnerable from stable atherosclerotic plaques? *Mol Imaging.* (2013) 13:1–5. doi: 10.2310/7290.2013.00061
 83. Silvolta JMU, Li X-G, Virta J, Marjamäki P, Liljenbäck H, Hytönen JP, et al. Aluminum fluoride-18 labeled folate enables *in vivo* detection of atherosclerotic plaque inflammation by positron emission tomography. *Sci Rep.* (2018) 8:9720. doi: 10.1038/s41598-018-27618-4
 84. Hyafil F, Pelisek J, Laitinen I, Schottelius M, Mohring M, Yvonne D, et al. Imaging the cytokine receptor CXCR4 in atherosclerotic plaques with the radiotracer 68 Ga-pentixafor for PET. *J Nucl Med.* (2017) 58:499–506. doi: 10.2967/jnumed.116.179663
 85. Li X, Heber D, Leike T, Beitzke D, Lu X, Zhang X, et al. [68Ga]Pentixafor-PET/MRI for the detection of chemokine receptor 4 expression in atherosclerotic plaques. *Eur J Nucl Med Mol Imaging.* (2018) 45:558–66. doi: 10.1007/s00259-017-3831-0
 86. Weiberg D, Thackeray JT, Daum G, Sohns JM, Kropf S, Wester H-J, et al. Clinical molecular imaging of chemokine receptor CXCR4 expression in atherosclerotic plaque using 68 Ga-pentixafor PET: correlation with cardiovascular risk factors and calcified plaque burden. *J Nucl Med.* (2018) 59:266–72. doi: 10.2967/jnumed.117.196485
 87. Meester EJ, Krenning BJ, de Blois RH, Norenberg JP, de Jong M, Bernsen MR, et al. Imaging of atherosclerosis, targeting LFA-1 on inflammatory cells with 111In-DANBIRT. *J Nucl Cardiol.* (2018) 20:8:1–8. doi: 10.1007/s12350-018-1244-5
 88. Ye Y, Calcagno C, Binderup T, Courties G, Keliher EJ, Wojtkiewicz GR, et al. Imaging macrophage and hematopoietic progenitor proliferation in atherosclerosis. *Circ Res.* (2015) 117:835–45. doi: 10.1161/CIRCRESAHA.115.307024
 89. Liu Y, Pierce R, Luehmann HP, Sharp TL, Welch MJ. PET imaging of chemokine receptors in vascular injury-accelerated atherosclerosis. *J Nucl Med.* (2013) 54:1135–41. doi: 10.2967/jnumed.112.114777
 90. Luehmann HP, Detering L, Fors BP, Pressly ED, Woodard PK, Randolph GJ, et al. PET/CT imaging of chemokine receptors in inflammatory atherosclerosis using targeted nanoparticles. *J Nucl Med.* (2016) 57:1124–9. doi: 10.2967/jnumed.115.166751
 91. Luehmann HP, Pressly ED, Detering L, Wang C, Pierce R, Woodard PK, et al. PET/CT Imaging of chemokine receptor CCR5 in vascular injury model using targeted nanoparticle. *J Nucl Med.* (2014) 55:629–34. doi: 10.2967/jnumed.113.132001
 92. Li D, Patel AR, Klibanov AL, Kramer CM, Ruiz M, Kang BY, et al. Molecular imaging of atherosclerotic plaques targeted to oxidized LDL receptor LOX-1 by SPECT/CT and magnetic resonance. *Circ Cardiovasc Imaging.* (2010) 3:464–72. doi: 10.1161/CIRCIMAGING.109.896654
 93. De Vos J, Mathijs I, Xavier C, Massa S, Wernery U, Bouwens L, et al. Specific Targeting of atherosclerotic plaques in ApoE-/ mice using a new camelid sdAb binding the vulnerable plaque marker LOX-1. *Mol Imaging Biol.* (2014) 16:690–8. doi: 10.1007/s11307-014-0731-6
 94. Pugliese F, Gaemperli O, Kinderlerer AR, Lamare F, Shalhoub J, Davies AH, et al. Imaging of vascular inflammation with [11C]-PK11195 and positron emission tomography/computed tomography angiography. *J Am Coll Cardiol.* (2010) 56:653–61. doi: 10.1016/j.jacc.2010.02.063
 95. Gaemperli O, Shalhoub J, Owen DRJ, Lamare F, Johansson S, Fouladi N, et al. Imaging intraplaque inflammation in carotid atherosclerosis with 11C-PK11195 positron emission tomography/computed tomography. *Eur Heart J.* (2012) 33:1902–10. doi: 10.1093/euroheartj/eht367
 96. Hellberg S, Liljenbäck H, Eskola O, Morisson-Iveson V, Morrison M, Trigg W, et al. Positron emission tomography imaging of macrophages in atherosclerosis with 18 F-GE-180, a radiotracer for translocator protein (TSPO). *Contrast Media Mol Imaging.* (2018) 2018:1–11. doi: 10.1155/2018/9186902
 97. Nahrendorf M, Zhang H, Hembrador S, Panizzi P, Sosnovik DE, Aikawa E, et al. Nanoparticle PET-CT imaging of macrophages in inflammatory atherosclerosis. *Circulation.* (2008) 117:379–87. doi: 10.1161/CIRCULATIONAHA.107.741181
 98. Keliher EJ, Ye YX, Wojtkiewicz GR, Aguirre AD, Tricot B, Senders ML, et al. Polyglucose nanoparticles with renal elimination and macrophage avidity facilitate PET imaging in ischaemic heart disease. *Nat Commun.* (2017) 8:1–12. doi: 10.1038/ncomms14064
 99. De Saint-Hubert M, Bauwens M, Deckers N, Drummen M, Douma K, Granton P, et al. *In vivo* molecular imaging of apoptosis and necrosis in atherosclerotic plaques using MicroSPECT-CT and MicroPET-CT imaging. *Mol Imaging Biol.* (2014) 16:246–54. doi: 10.1007/s11307-013-0677-0
 100. Liu Z, Larsen BT, Lerman LO, Gray BD, Barber C, Hedyat AF, et al. Detection of atherosclerotic plaques in ApoE-deicient mice using 99m Tc-duramycin. *Nucl Med Biol.* (2016) 43:496–505. doi: 10.1016/j.nucmedbio.2016.05.007
 101. Hu Y, Liu G, Zhang H, Li Y, Gray BD, Pak KY, et al. A comparison of [99mTc]Duramycin and [99mTc]annexin V in SPECT/CT imaging atherosclerotic plaques. *Mol Imaging Biol.* (2018) 20:249–59. doi: 10.1007/s11307-017-1111-9
 102. Razavian M, Marfatia R, Mongue-Din H, Tavakoli S, Sinusas AJ, Zhang J, et al. Integrin-targeted imaging of inflammation in vascular remodeling. *Arterioscler Thromb Vasc Biol.* (2011) 31:2820–6. doi: 10.1161/ATVBAHA.111.231654
 103. Paeng JC, Lee YS, Lee JS, Jeong JM, Kim KB, Chung JK, et al. Feasibility and kinetic characteristics of 68Ga-NOTA-RGD PET for *in vivo* atherosclerosis imaging. *Ann Nucl Med.* (2013) 27:847–54. doi: 10.1007/s12149-013-0757-x
 104. Su H, Gorodny N, Gomez LF, Gangadharam UB, Mu F, Chen G, et al. Atherosclerotic plaque uptake of a novel integrin tracer 18 F-Flotegatide in a mouse model of atherosclerosis. *J Nucl Cardiol.* (2015) 21:553–62. doi: 10.1007/s12350-014-9879-3
 105. Laitinen I, Saraste A, Weidl E, Poethko T, Weber AW, Nekolla SG, et al. Evaluation of $\alpha\beta$ integrin-targeted positron emission tomography tracer 18F-galacto-RGD for imaging of vascular inflammation

- in atherosclerotic mice. *Circ Cardiovasc Imaging*. (2009) 2:331–8. doi: 10.1161/CIRCIMAGING.108.846865
106. Beer AJ, Pelisek J, Heider P, Saraste A, Reeps C, Metz S, et al. PET/CT imaging of integrin $\alpha v\beta 3$ expression in human carotid atherosclerosis. *JACC Cardiovasc Imaging*. (2014) 7:178–87. doi: 10.1016/j.jcmg.2013.12.003
 107. Jiang L, Tu Y, Kimura RH, Habte F, Chen H, Cheng K, et al. 64Cu-labeled divalent cystine knot peptide for imaging carotid atherosclerotic plaques. *J Nucl Med*. (2015) 56:939–44. doi: 10.2967/jnumed.115.155176
 108. Vancraeynest D, Roelants V, Bouzin C, Hanin F, Walrand S, Bol V, et al. $\alpha V\beta 3$ integrin-targeted microSPECT / CT imaging of inflamed atherosclerotic plaques in mice. *EJNMMI Res*. (2016) 6:29. doi: 10.1186/s13550-016-0184-9
 109. Sun Yoo J, Lee J, Ho Jung J, Seok Moon B, Kim S, Chul Lee B, et al. SPECT/CT imaging of high-risk atherosclerotic plaques using integrin-binding RGD dimer peptides. *Sci Rep*. (2015) 5:11752. doi: 10.1038/srep11752
 110. Tekabe Y, Kollaros M, Zhang G, Backer M V, Backer JM, Johnson LL. Imaging VEGF receptor expression to identify accelerated atherosclerosis. *EJNMMI Res*. (2014) 4:41. doi: 10.1186/s13550-014-0041-7
 111. Tekabe Y, Johnson LL, Rodriguez K, Li Q, Backer M, Backer JM. Selective imaging of vascular endothelial growth factor receptor-1 and receptor-2 in atherosclerotic lesions in diabetic and non-diabetic ApoE $-/-$ mice. *Mol Imaging Biol*. (2018) 20:85–93. doi: 10.1007/s11307-017-1045-2
 112. Razavian M, Nie L, Challa A, Zhang J, Golestanian R, Jung JJ, et al. Lipid lowering and imaging protease activation in atherosclerosis. *J Nucl Cardiol*. (2014) 21:319–28. doi: 10.1007/s12350-013-9843-7
 113. Tavakoli S, Razavian M, Zhang J, Nie L, Marfatia R, Dobrucki LW, et al. Matrix metalloproteinase activation predicts amelioration of remodeling after dietary modification in injured arteries. *Arterioscler Thromb Vasc Biol*. (2011) 31:102–9. doi: 10.1161/ATVBAHA.110.216036
 114. Zhang J, Nie L, Razavian M, Ahmed M, Dobrucki LW, Asadi A, et al. Molecular imaging of activated matrix metalloproteinases in vascular remodeling. *Circulation*. (2008) 118:1953–60. doi: 10.1161/CIRCULATIONAHA.108.789743
 115. Razavian M, Tavakoli S, Zhang J, Nie L, Dobrucki LW, Sinusasa J, et al. Atherosclerosis plaque heterogeneity and response to therapy detected by *in vivo* molecular imaging of matrix metalloproteinase activation. *J Nucl Med*. (2011) 52:1795–802. doi: 10.2967/jnumed.111.092379
 116. Bigalke B, Phinikaridou A, Andia ME, Cooper MS, Schuster A, Schönberger T, et al. Positron emission tomography/computed tomographic and magnetic resonance imaging in a murine model of progressive atherosclerosis using 64Cu-labeled glycoprotein VI-Fc. *Circ Cardiovasc Imaging*. (2013) 6:957–64. doi: 10.1161/CIRCIMAGING.113.000488
 117. Nakamura I, Hasegawa K, Wada Y, Hirase T, Node K, Watanabe Y. Detection of early stage atherosclerotic plaques using PET and CT fusion imaging targeting P-selectin in low density lipoprotein receptor-deficient mice. *Biochem Biophys Res Commun*. (2013) 433:47–51. doi: 10.1016/j.bbrc.2013.02.069
 118. Li X, Bauer W, Israel I, Kreissl MC, Weirather J, Richter D, et al. Targeting P-selectin by gallium-68-labeled fucoidan positron emission tomography for noninvasive characterization of vulnerable plaques: correlation with *in vivo* 17.6T MRI. *Arterioscler Thromb Vasc Biol*. (2014) 34:1661–7. doi: 10.1161/ATVBAHA.114.303485
 119. Broisat A, Hernot S, Toczek J, De Vos J, Riou LM, Martin S, et al. Nanobodies targeting mouse/human VCAM1 for the nuclear imaging of atherosclerotic lesions. *Circ Res*. (2012) 110:927–37. doi: 10.1161/CIRCRESAHA.112.265140
 120. Broisat a., Toczek J, Dumas LS, Ahmadi M, Bacot S, Perret P, et al. 99mTc-cAbVCAM1-5 imaging is a sensitive and reproducible tool for the detection of inflamed atherosclerotic lesions in mice. *J Nucl Med*. (2014) 55:1678–84. doi: 10.2967/jnumed.114.143792
 121. Dumas LS, Briand F, Clerc R, Brousseau E, Montemagno C, Ahmadi M, et al. Evaluation of antiatherogenic properties of ezetimibe using 3 H-labeled low-density-lipoprotein cholesterol and 99m Tc-cAbVCAM1-5 SPECT in ApoE $-/-$ mice fed the paigen diet. *J Nucl Med*. (2017) 58:1088–93. doi: 10.2967/jnumed.116.177279
 122. Bala G, Blykers A, Xavier C, Descamps B, Broisat A, Ghezzi C, et al. Targeting of vascular cell adhesion molecule-1 by 18 F-labelled nanobodies for PET/CT imaging of inflamed atherosclerotic plaques. *Eur Hear J Cardiovasc Imaging*. (2016) 17:1001–8. doi: 10.1093/eihjci/jev346
 123. Nahrendorf M, Kelher E, Panizzi P, Zhang H, Hembrador S, Figueiredo J-L, et al. 18F-4V for PET-CT imaging of VCAM-1 expression in atherosclerosis. *JACC Cardiovasc Imaging*. (2009) 2:1213–22. doi: 10.1016/j.jcmg.2009.04.016
 124. Mateo J, Izquierdo-Garcia D, Badimon JJ, Fayad ZA, Fuster V. Noninvasive assessment of hypoxia in rabbit advanced atherosclerosis using 18 f-fluoromisonidazole positron emission tomographic imaging. *Circ Cardiovasc Imaging*. (2014) 7:312–20. doi: 10.1161/CIRCIMAGING.113.001084
 125. Hag AMF, Ripa RS, Pedersen SF, Bodholdt RP, Kjaer A. Small animal positron emission tomography imaging and *in vivo* studies of atherosclerosis. *Clin Physiol Funct Imaging*. (2013) 33:173–85. doi: 10.1111/cpf.12017
 126. Quillard T, Libby P. Molecular imaging of atherosclerosis for improving diagnostic and therapeutic development. *Circ Res*. (2012) 111:231–44. doi: 10.1161/CIRCRESAHA.112.268144
 127. Ridker PM, Everett BM, Thuren T, MacFadyen JG, Chang WH, Ballantyne C, et al. Antiinflammatory therapy with canakinumab for atherosclerotic disease. *N Engl J Med*. (2017) 377:1119–31. doi: 10.1056/NEJMoa1707914
 128. Kottoor SJ, Arora RR. The utility of anti-inflammatory agents in cardiovascular disease. *J Cardiovasc Pharmacol Ther*. (2018) 23:483–93. doi: 10.1177/1074248418778548
 129. Sarikaya I, Larson SM, Freiman A, Strauss HW. What nuclear cardiology can learn from nuclear oncology. *J Nucl Cardiol*. (2003) 10:324–8. doi: 10.1016/S1071-3581(03)00521-X
 130. Carlier T, Baily C. State-of-the-art and recent advances in quantification for therapeutic follow-up in oncology using PET. *Front Med*. (2015) 2:1–12. doi: 10.3389/fmed.2015.00018
 131. van der Vos CS, Koopman D, Rijnsdorp S, Arends AJ, Boellaard R, van Dalen JA, et al. Quantification, improvement, and harmonization of small lesion detection with state-of-the-art PET. *Eur J Nucl Med Mol Imaging*. (2017) 44:4–16. doi: 10.1007/s00259-017-3727-z

Conflict of Interest Statement: The authors declare that the research was conducted in the absence of any commercial or financial relationships that could be construed as a potential conflict of interest.

Copyright © 2019 Meester, Krenning, de Swart, Segbers, Barrett, Bernsen, Van der Heiden and de Jong. This is an open-access article distributed under the terms of the Creative Commons Attribution License (CC BY). The use, distribution or reproduction in other forums is permitted, provided the original author(s) and the copyright owner(s) are credited and that the original publication in this journal is cited, in accordance with accepted academic practice. No use, distribution or reproduction is permitted which does not comply with these terms.